JOURNAL OF CATALYSIS 87, 66–76 (1984)

The Catalytic Reduction of Carbon Monoxide over Iron Surfaces: A Surface Science Investigation

D. J. DWYER AND J. H. HARDENBERGH

Exxon Research and Engineering, Corporate Research Science Laboratory, Route 22 East, Annandale, New Jersey 08801

Received May 25, 1983; revised December 22, 1983

The hydrogenation of carbon monoxide over iron surfaces has been investigated at medium pressure (7 atm) and over the temperature range 473–578 K. The study was performed in ultrahigh vacuum surface analytical system equipped with a high-pressure reactor capability. High-purity iron foils were found to deactivate rapidly under synthesis conditions. This deactivation appears to be associated with the deposition of a graphitic type of surface carbon. Under the same reaction conditions higher surface area iron powders promote the formation of carbidic rather than graphitic carbon. The carbided surfaces were more stable under reaction conditions but were also susceptible to poisoning by graphite deposition at temperature above 550 K. Changes in catalyst activity and selectivity can be correlated with changes in the amount and type of carbon on the surface.

INTRODUCTION

The reduction of carbon monoxide over iron catalysts has been investigated extensively over the past 60 years. Since the discovery by Fischer and Tropsch in 1923 (*1*) that alkalized iron fillings produced liquid and solid hydrocarbons, iron-based catalysts have been the mainstay of hydrocarbon synthesis. Over the years, the iron catalyst has evolved into two major forms: the precipitated iron catalyst and the fused ammonia synthesis-type catalyst. The precipitated catalyst is a high-surface-area (400 m^2/g) iron oxide (Fe_2O_3) used in fixed beds to produce high-molecular-weight hydrocarbons (*2*). The fused iron catalyst is a lower surface area (70–100 m^2/g) but a higher mechanical strength iron oxide (Fe_3O_4). The fused catalyst is used in fluidized beds to produce molecules in the motor fuel range. Both catalysts, in addition to iron oxide, contain copper and difficult-to-reduce oxides of potassium, zinc, or silicon. The copper and silicon dioxide are added to stabilize the surface area of the catalyst during reduction. Silicon dioxide acts as a physical barrier against particle sintering which preserves pore structure (*3*). Copper lowers the temperature necessary for reduction which also inhibits sintering. Potassium is added as either K_2O or K_2CO_3 to lower the methane yield and to shift the distribution of products to higher molecular weights.

In spite of the extensive literature dealing with iron catalysts, confusion remains as to the exact nature of the working catalytic surface. In part, this is due to the wide variety of catalyst preparations and the fact that the working catalyst often contains a mixture of iron oxides, iron carbides, and a small amount of α-iron (*4, 5*). The extent to which these phases are present depends on catalyst pretreatment, conversion levels, temperature, and H_2/CO ratio. To date, there is no clear consensus as to which of these phases is responsible for catalyst activity. For example, Raupp and Delgass (*6*) and Niemantsverdriet *et al.* (*7*) have demonstrated a positive correlation between the extent of carbide formation and the activity of the catalyst. In contrast Teichner and coworkers (*8*) suggest that iron carbide is a

0021-9517/84 $3.00

noncatalyst and is rapidly deactivated under synthesis conditions. They find iron oxides are necessary components of the working catalyst. Surface science experiments by Bonzel (*9*) and others (*10*) have shown that metallic iron is catalytically active but is very susceptible to poisoning by carbon deposition. A high hydrogen-to-carbon-monoxide ratio in the reactant stream is necessary to keep the surface active. Bonzel and Krebs (*9, 11, 13*) suggest a model for the iron catalyst similar to that proposed by Goodman *et al.* (*14*) for nickel catalysts. The main feature of the model is that carbon monoxide dissociation on the metallic surface is the major pathway to hydrocarbon formation. The dissociation step produces a highly active surface carbon species with an electronic structure similar to surface carbide. Competition between the hydrogenation of the active carbon and its decomposition into surface graphite (inactive) determines the catalyst lifetime. It is interesting to note that Bonzel and Krebs report that potassium, while decreasing the amount of methane, accelerates the deactivation of the surface by surface graphite (*12, 15*).

The present study was undertaken in an attempt to identify which phases of the iron, carbon, oxygen system are active for carbon monoxide reduction. The approach we have taken is to study a variety of well-characterized iron surfaces in a medium-pressure (1–10 atm) microreactor directly attached to an ultrahigh vacuum surface analysis system. The purpose of these experiments was to measure the intrinsic catalytic response of various unpromoted iron surfaces. To minimize the number of variables, the study was performed at ultralow conversion, with fixed hydrogen-to-carbon-monoxide ratio and total pressure. Only temperature and conversion were allowed to vary. This publication deals with our results over metallic iron surfaces; subsequent papers will deal with iron oxides and potassium-promoted surfaces.

EXPERIMENTAL METHOD

The experimental system has been described elsewhere (*16*). It consists of a medium-pressure microreactor coupled directly to a Leybold–Hereaus surface analysis system. The reactor and transfer device is similar in concept to that used by Bonzel and co-workers (*9*) but with one major difference. Rather than rely on resistive heating of our catalysts we have designed the reactor as a small-volume (>10 cc) gold-plated tube furnace. This design ensures that both the gas and sample are isothermal and that good mixing of the gas takes place in the reactor. The samples used in this study were high-purity iron foils (5 *N*) and high-purity iron powders formed by reduction of ultrahigh purity Fe_2O_3 (Baker). The samples were mounted on a gold sample boat which could be manipulated from outside the vacuum system by magnetic motion feedthroughs. This system permits the removal of the sample from the reactor directly to the ultrahigh vacuum chamber.

The gases used in the study were purchased premixed in aluminum cylinders. The high-purity gas mixture (5 *N*) was further purified by use of a in-line zeolite water trap and a copper carbonyl trap. The gas pressure in the reactor was measured with a capacitance manometer and the flow controlled by a Tylan mass flow controller. The typical flow rate was 15 cc/min (STP) and the maximum conversion was $\approx 1\%$ based on integration of the hydrocarbon product. The reaction products were analyzed by gas chromatography (temperature-programmed Chromsorb 102, FID, and TCD detectors).

X-Ray photoelectron spectra were measured with a pass energy of 50 eV and aluminum K_α radiation. The spectrometer work function and the gain on the high voltage amplifier were calibrated by setting the binding energy of the Cu $2p^{3/2}$ at 932.8 eV and the Cu 3*s* at 122.9 eV. All XPS binding

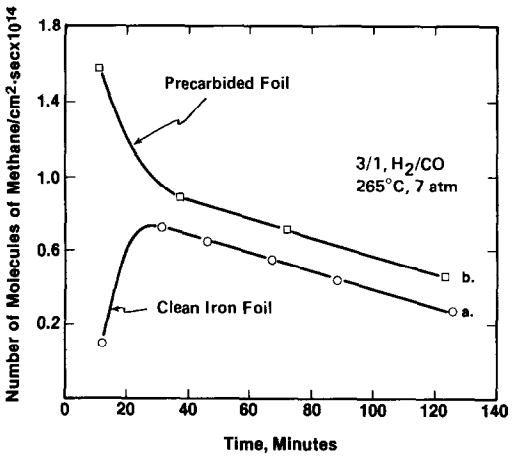

FIG. 1. Rate of methane formation as a function of time at 265°C, 7 atm, 3/1 H_2/CO. Curve a, clean iron foil; curve b, precarbided foil.

energies are referenced to the iron Fermi level.

RESULTS

Iron Foil Experiments

The catalytic reduction of carbon monoxide was studied over high-purity iron foils at 533 K (260°C), 730 kPa (7 atm), H_2/CO ratio 3/1, and a feed rate of 15 cc/min. The iron sample was cleaned in ultrahigh vacuum by argon ion sputtering to remove residual surface oxide. The sample was then moved directly into the reactor system and exposed to CO/H_2. The reactor was brought to temperature (≈10 min) and product analysis started. Curve a in Fig. 1 demonstrates the catalytic response of an atomically clean iron surface. The major reaction product under our conditions was methane (70 mole %) but small amounts of larger hydrocarbons (up to C_5) were detected. These hydrocarbons were mainly linear paraffins. No alcohols or other oxygenated hydrocarbons were detected. As shown in Fig. 1, curve a, the catalytic activity goes through a maximum after approx 25 min under reaction conditions. If an iron site density of $10^{15} \cdot cm^{-2}$ is assumed then the maximum rate corresponds to a turnover frequency of 0.1 molecule · site^{-1} · sec^{-1}. This value is in reasonable agreement (considering the reported range, 0.05–2.0) with previous studies over iron foils (*9, 10, 17*). Beyond the maximum, the rate decreases monotonically and finally drops below the detectability limit of our system after 3 hr.

X-Ray photoelectron spectra of the foil before and after reaction with CO/H_2 revealed information concerning the catalytic response of the foil. These results are summarized by the spectra in Fig. 2. Spectra A in Fig. 2 was obtained after ion sputtering. The binding energy of the Fe $2p^{3/2}$ line was 706.6 eV in excellent agreement with previous results (*18*). The only surface impurity detected after sputtering was a small amount of residual carbon characterized by a C 1*s* peak centered at E_b = 284.6 eV. After reaction as shown in Fig. 2B, a highly reproducible shift in the Fe $2p^{3/2}$ binding energy from 706.6 to 706.9 eV was observed. A concommitant increase in the intensity and the appearance of two peaks in the C 1*s* region were observed. We interpret these carbon lines in the following manner. The shift toward higher binding energy in the Fe

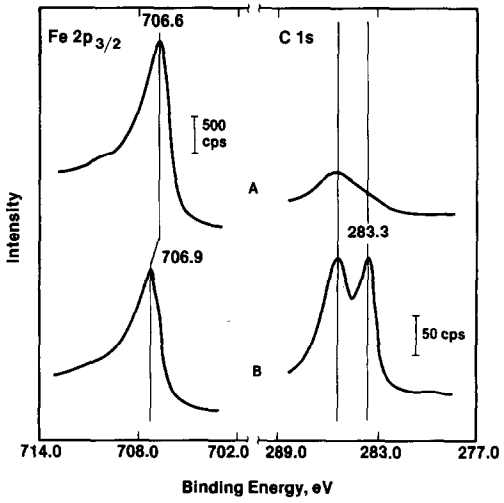

FIG. 2. Fe $2p^{3/2}$ and C 1*s* XPS spectra of iron foil (a) after UHV cleaning and (b) after reaction (265°C, 7 atm, 3/1 H_2/CO).

TABLE 1

Binding Energy for Various Carbon Species

Species	Present	Ref. (*11*)
High-purity graphite	284.6	—
Graphite on Fe foil	284.6	285.0
Surface carbide	283.3	283.3
CH_x on Fe foil[a]	285.8	283.9

[a] Carbonaceous deposit prepared by melting a small amount of octocosane (C_{28}) on a iron foil. Bonzel and Krebs (*11*) used gaseous ethylene to prepare the CH_x deposit.

$2p^{3/2}$ line coupled with the appearance of a low-binding-energy form of carbon (E_b = 283.3 eV) strongly suggests the formation of a carbide phase within the surface region. The second carbon feature (E_b = 284.6 eV) is assigned to a graphitic surface deposit. The assignment is based on binding energies measured in our laboratory for various standards as shown in Table 1.

The results obtained in these experiments are in general agreement with those of Bonzel and Krebs (*9*, *11*). As correctly pointed out by Bonzel the deactivation of the iron surface can be correlated with the deposition of surface graphite. This fact was demonstrated in the present study in the following manner. First, an iron foil was precarbided by treating with CO/H_2 under the standard conditions. Then the sample was lightly ion sputtered in ultrahigh vacuum to remove the majority of the surface graphite. This preferential removal of surface graphite (E_b = 284.6 eV) is demonstrated in Fig. 3a. The catalytic response of this precarbided iron foil is shown in Fig. 1b. The rate of methanation quickly rises to a maximum value of approx 1.5×10^{14} molecules $\cdot$ cm^{-2} $\cdot$ sec^{-1} followed once again by a monotonic decrease in activity. The C 1*s* spectrum in Fig. 3b clearly shows that the deactivation is correlated with the buildup of graphitic carbon on the surface.

Although the results of these foil experiments are in good agreement with previous experiments with foils, they do not agree with experiments over higher surface area iron. The catalytic lifetime of the foil is much shorter than that of iron powders (*7*, *8*). The product distribution (70% methane) is also not typical of unpromoted iron catalysts. To explore these discrepancies we have experimented with a higher surface area sample.

Metallic Iron Powders

In this series of experiments, a fused iron powder sample was prepared in the following manner. First, a high-purity iron oxide (α-Fe_2O_3) was totally reduced (723 K, 100 kPa, H_2, 8 hr) in an external tube furnace. This pyrophoric iron powder was passivated by exposure to 1% O_2 in He for 2 hr at room temperature. A 20-mg sample of the passivated material was fused in a pellet press into a porous wafer. The standard

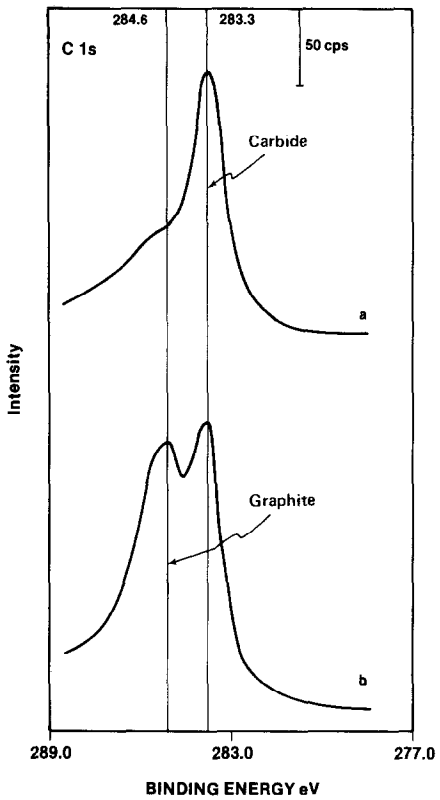

FIG. 3. Carbon 1*s* XPS spectra of precarbided foil (a) before reaction and (b) after reaction (265°C, 7 atm, 3/1 H_2/CO).

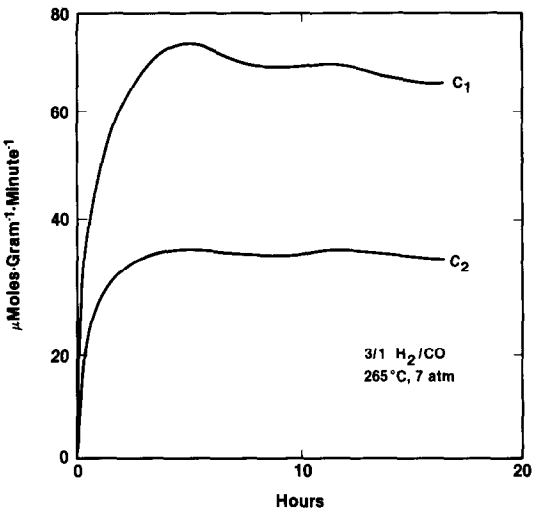

FIG. 4. Rate of methane and ethane production over iron powder as a function of time at 265°C, 7 atm, 3/1 H_2/CO.

BET surface area of the material after pressing was ≈16 m^2/g. The wafer was then mounted in the spectrometer–reactor system.

XPS studies of the passivated higher surface area iron sample revealed that the surface was predominantly Fe_2O_3 (*19*), although X-ray diffraction indicated only α-Fe was present in the bulk. This result suggests that the iron powder is covered by a thin (<100 Å) oxide skin. This residual oxide could be removed easily by H_2 reduction (2 hr, 623 K, 2 atm). The only detectable impurities by XPS was a small amount of sulfur and carbon. These impurities occupied no more than 1% of the surface region.

After characterization, the powder sample was moved directly into the reactor system and brought to standard reaction conditions (730 kPa, 3/1 H_2/CO, 533 K). The catalytic response of this material as shown in Fig. 4 was substantially different than that of the iron foils. Rather than rapid deactivation the activity of this material accelerated with time and eventually reached a steady state after 3 hr of reaction. The methanation rate at this point was ≈78 $\mu moles \cdot g^{-1} \cdot min^{-1}$. The total CO conversion to hydrocarbons was ≈2%. The product distribution for the reaction after steady sate was achieved is given in Fig. 5. In addition to the C_1 to C_6 hydrocarbons shown in Fig. 5 trace amounts of C_7 and C_8 were observed. The product distribution obtained over these samples was quite different than that observed over the iron foils. The meth-

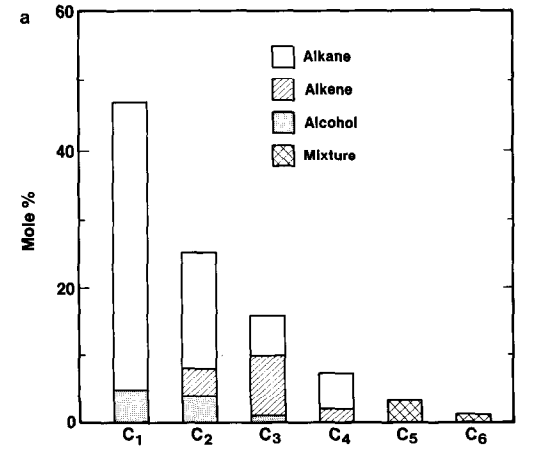

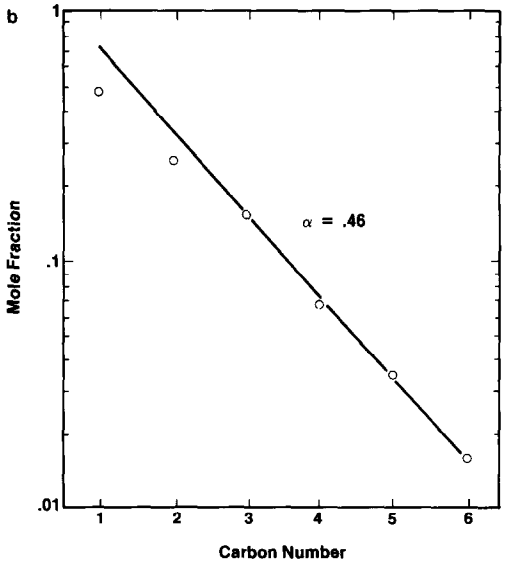

FIG. 5. Product distribution at steady state over iron powder at 265°C, 7 atm, 3/1 H_2/CO: (a) product distribution; (b) Schultz–Flory plot.

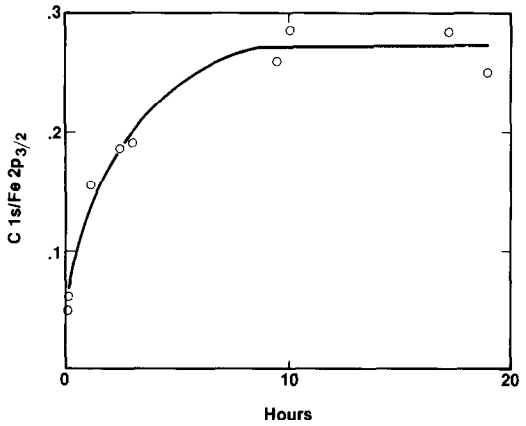

FIG. 6. Surface carbon accumulation as a function of time on iron powder under CO/H_2 (265°C, 7 atm, 3/1 H_2/CO).

ane yield was lower (42 mole % vs 70 mole %) and appreciable quantities of alcohols and alkenes were detected. A Flory-type (*20*) analysis of the hydrocarbon distribution is given in Fig. 5b. Following the method of Satterfield and Huff (*21*), we have included the oxygenated hydrocarbons into the analysis. A linear least squares fit of the data yields a chain growth probability parameter $\alpha = 0.46$ (*9, 20, 21*). It should be noted that even when both methanol and ethanol are added to the C_1 and C_2 fractions, these components fall below the Flory line.

Surface analysis of the iron catalyst as a function of time under CO/H_2 reveals that extensive carbon deposition occurs on the surface of the material. Figure 6 demonstrates the buildup of carbon as a function of reaction time. By comparing Figs. 4 and 6 it appears that a qualitative correlation can be made between the accumulation of carbon on the surface and the catalytic activity. To probe this further, high-resolution (20-eV pass energy) XPS spectra were recorded at various points into the reaction. The results are shown in Fig. 7. Early in the reaction the surface region is quickly carbided as indicated by the intense C 1*s* feature centered at 283.3 eV and the shift of the Fe $2p^{3/2}$ to 706.9 eV. The carbide content of the surface increases with time over the first 2 hr of reaction while the concomitant catalytic activity is also increasing. Beyond the 2-hr mark a small amount of surface graphite is also deposited on the catalyst but the ratio of graphite to carbide is nowhere near the levels observed on the iron foils.

Temperature Response of the Reaction

One advantage of the iron powder samples over the iron foils is the achievement of the stable reaction kinetics after carbidation of the surface. This kinetic stability permits the investigation of the temperature dependence of the reaction. To explore this dependence, we varied the temperature over the range 473 K (200°C) to 578 K (305°C). The total pressure and gas flow were held constant but the conversion was

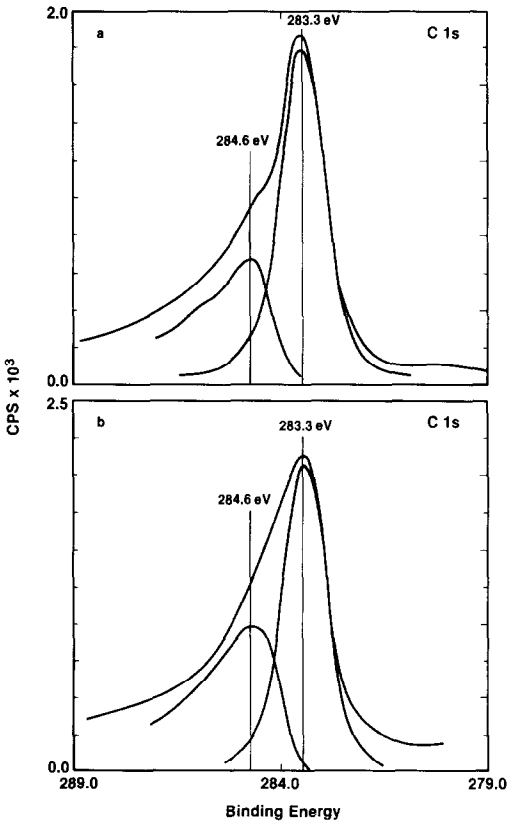

FIG. 7. Carbon 1*s* XPS spectra from iron powder (a) 1 hr under CO/H_2 and (b) after 5 hr under CO/H_2.

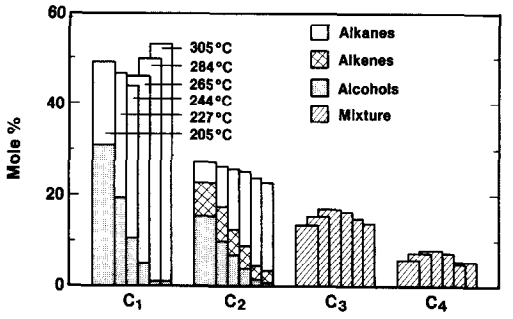

FIG. 8. Product distribution from iron powder as a function of temperature at 7 atm 3/1 H_2/CO.

allowed to vary with temperature. The reactor system was stabilized for at least 2.5 hr at each temperature investigated.

The influence of temperature on the product distribution is shown in Fig. 8. These trends are observed. First, the overall distribution of molecules is relatively stable with temperature. This suggests an insensitivity of the chain growth probability to temperature under our reaction conditions. Second, as the temperature is lowered the relative amounts of alcohols and alkenes increase. In fact, at 478 K (205°C), almost 45% of the molecules produced are alcohols. Third, the hydrogenation activity of the catalyst rapidly increases with temperature as indicated by the decrease in the ethylene-to-ethane ratio and the increase in methane yield. The increase in methane yield occurs primarily at the expense of methanol and, to a lesser degree, the higher molecular weight products.

In an attempt to measure the apparent activation energies for the various products, the kinetics were also measured as a function of temperature. The results of these measurements for methane and ethane are shown in an Arrhenius format in Figs. 9 and 10. In the case of methane the rate varied from 2.4 μmoles $\cdot$ g^{-1} $\cdot$ min^{-1} at 478 K (205°C) to greater than 3.5×10^2 μmoles $\cdot$ g^{-1} $\cdot$ min^{-1} at 578 K (305°C). The variation with temperature yields an apparent activation energy of E_a = 29.9 kcal $mole^{-1}$. This value is higher than that reported elsewhere (*9, 10, 17*). This discrepancy may be due to the fact that the present samples were fully carbided. The rate of ethane production over this same temperature range varied from 0.64 to 129 μmoles $\cdot$ g^{-1} $\cdot$ min^{-1} as shown in Fig. 10. The apparent activation energy for ethane is 30.0 kcal $mole^{-1}$.

During these kinetic measurements it was found that the catalyst would not stabilize at temperatures above 573 K (300°C) but began to deactivate with time. This deactivation process was studied by allowing the catalyst to remain at 578 K (305°C) for 16 hr. The catalytic activity of the system dropped about 50% during this time interval. This drop in activity is depicted by the

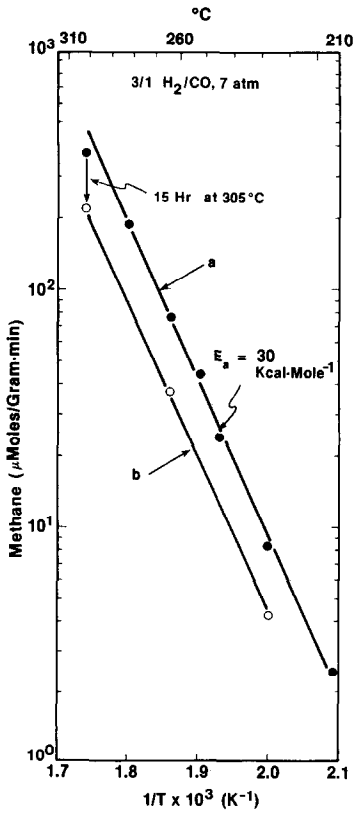

FIG. 9. Arrhenius plot for methane formation over iron powder, E_a = 29.9 kcal-$mole^{-1}$ (a) before high-temperature carbon deposition and (b) after carbon poisoning. Arrow indicates drop in rate during a 15-hr period to 305°C.

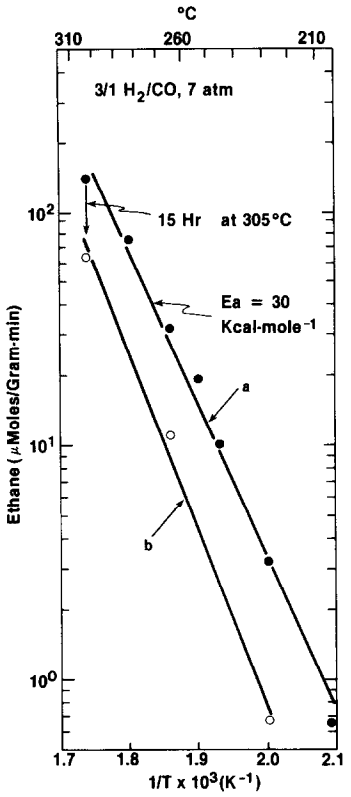

FIG. 10. Arrhenius plot for ethane formation over iron powder, E_a = 30.0 kcal-mole^{-1}; (a) and (b), same as Fig. 9.

arrows in Figs. 9 and 10. The catalyst was removed from the reactor after this period of deactivation and the surface investigated by XPS. As might be anticipated XPS revealed extensive carbon deposition had occurred on the catalyst during this time period. The position and lineshape of the C 1*s* feature (Fig. 11) reveals three types of carbon present on the poisoned surface: a weak carbide signal (283.3 eV), a weak carbonanceous signal (285.3 eV), and an intense graphite signal (284.6 eV). The graphitic carbon is the most likely cause of the catalyst deactivation. It is difficult to estimate the amount of carbon deposition at this point due to the porous nature of the substrate. However, the deposition is certainly in the multilayer regime due to the fact that the absolute intensity of the Fe $2p^{3/2}$ signal decreased by more than 50%.

DISCUSSION

Over the past several years there has been growing experimental evidence that the reduction of carbon monoxide proceeds through a surface carbide mechanism of the type originally proposed by Fischer and Tropsch (*22*) in 1926 and not through an oxygen-containing intermediate (*5*). The work of Araki and Ponec (*23*) and Biloen *et al.* (*24*) with carbon-13-labeled CO showed that surface carbon could be directly hydrogenated to hydrocarbons in the absence of CO. The work of Goodman and co-workers (*14*) demonstrated that the active form of carbon on a nickel surface is carbidic in nature and can be readily hydrogenated. Bonzel and Krebs (*9*) found similar results for iron. Finally, the work of Brady and Pettit (*25, 26*) showed that methylene (CH_2) can polymerize in the absence of CO over a variety of transition metal surfaces. The polymerization process leads to products similar to those observed under F–T conditions.

The general mechanism which has emerged from these studies and others has been reviewed by Biloen and Sachtler (*27*). The mechanism suggests that carbon monoxide and hydrogen are dissociatively

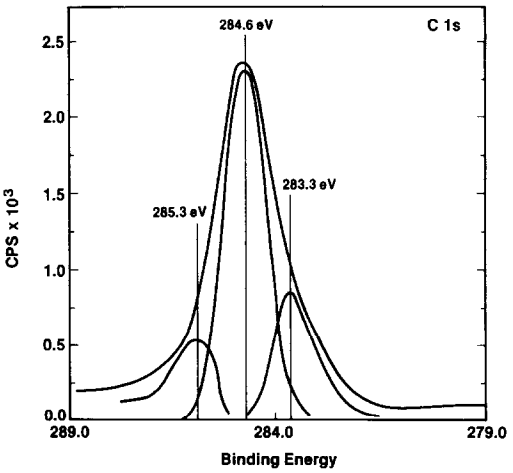

FIG. 11. Carbon 1*s* spectrum after high-temperature carbon deposition.

chemisorbed on the catalyst surface as atomic hydrogen, carbon, and oxygen:

$$(CO)_g \rightarrow C_s + O_s, \quad (1)$$

$$(H_2)_g \rightarrow 2H_s. \quad (2)$$

Oxygen is then rapidly removed from the surface through the reaction with atomic hydrogen to produce water:

$$O_s + 2H_s \rightarrow (H_2O)_g. \quad (3)$$

The key to catalytic response of the system is the fate of the highly reactive carbon species on the surface which can follow at least three reaction channels. It can diffuse into the metal and form a bulk carbide,

$$C_s + xM \rightarrow M_xC, \quad (4)$$

or it can react with other surface carbon atoms to form an unreactive graphitic-type carbon,

$$nC_s \rightarrow C_n \quad \text{(graphite)} \quad (5)$$

(The question of whether this carbon has true three-dimensional grahitic structure or is some form of amorphous carbon is moot. The key feature in terms of the catalysis is that it is of low reactivity and contains little or no hydrogen.) The third reaction channel is the interaction of surface carbon with atomic hydrogen to form a C_1 intermediate (probably chemisorbed methylene). These single carbon atom

$$C_s + 2H_s \rightarrow (CH_2)_s \quad (6)$$

intermediates can undergo polymerization to form larger hydrocarbons or be hydrogenated to methane:

$$n(CH_2) \rightarrow C_nH_{2n}, \quad (7)$$

$$CH_2 + 2H \rightarrow CH_4. \quad (8)$$

Most of the results reported in this paper can be interpreted within the framework of the surface carbide model. For example, the time dependence of the catalytic response of either the iron foils (Fig. 1) or iron powders (Fig. 4) can be explained in terms of the carbide competition model (*28*) of Niemantsverdriet and van der Kraan. This model suggests that a competition for surface carbon between carbidation of the iron (reaction (4)) and the hydrogenation to hydrocarbons (reactions (6)–(8)) results in the induction period observed over iron catalysts. The good correlation between overall activity and the amount of surface carbide as shown in Figs. 4 and 6 clearly suggest that steady state activity is only achieved after complete carbidation of the surface region. This competition between carbidation and hydrogenation is also demonstrated in Fig. 1 where the response of the atomically clean and precarbided iron foils is compared. The initial rates over the precarbided surface are a factor of 5 higher than those over the clean surface. This enhancement is most likely due to the removal of the carbidation channel on the precarbided samples. In the foil experiments it appears that graphite deposition (reaction (5)) dominates the kinetics and leads to rapid deactivation of the sample. In the case of the iron powder, the carbiding reaction is the dominate channel in the early part of the reaction and the hydrogenation reactions dominates in the later parts of the run. It is not apparent why these two similar systems respond differently but it may be associated with the low rates of carbidation of large iron particles (*29*).

The molecules produced over the iron powders (Fig. 5) are mainly small alkanes. Although some chain building (polymerization) takes place ($\alpha = 0.46$) the product distribution in these experiments is not typical of true Fischer–Tropsch chemistry ($\alpha > 0.65$) where the majority of products are liquid and solid hydrocarbons. This difference is undoubtedly due to the absence of alkali in these catalysts but it is also clear that the unpromoted iron or iron carbide surface is a poor catalyst. The low selectivity of these phases is probably due to the high hydrogenation activity of their surfaces. An excess concentration of chemisorbed hydrogen on the surface relative to C_1 intermediates would result in the interception and termination of growing chains on the surface.

One product which is not consistent with the carbide model is methanol. As shown in Fig. 8, methanol is approximately 5% of the total product at 538 K (265°C) but is the dominate product (32 mole %) at 478 K (205°C). Proponents of the carbide theory (*27*) generally explain alcohol production in terms of an alternative termination step involving the insertion of molecular CO into the growing chains. Methanol cannot be produced in this manner. However, it is possible to include methanol production by assuming that methanol is produced by the direct hydrogenation of molecular CO on the surface. The temperature response of the product distribution can then be rationalized in the following manner. At higher temperatures, the residence time of molecular CO becomes very short and the major mode of CO chemisorption is dissociative. This dissociated CO would lead to hydrocarbon production as outlined above. At the lower temperatures, molecular CO could become a major component on the iron carbide surface leading to the higher levels of methanol observed. Since CO can efficiently compete with hydrogen chemisorption at these lower temperatures, this increase in molecular CO and concomitant decrease in atomic hydrogen on the surface could also explain the increase in the ethylene-to-ethane ratio.

An alternative explanation for the enhanced methanol production at lower temperatures is that methanol is a primary product (*5*) and arises from a common intermediate with methane. At low temperature (low conversion), the probability of methanol decomposition through a secondary reaction would decrease thus explaining the increased amounts of methanol observed. This secondary reaction could be dissociation back to CO and H_2 or a dehydration reaction to form the C_1 equivalent of an alkene, namely, methylene. This linking of methanol and methane through a common intermediate could explain the fact that the methane-to-methanol ratio varies rapidly with temperature but the total amount of C_1 does not (Fig. 8). We plan to investigate this interesting possibility that methanol and methane chemistry are linked by further studies.

ACKNOWLEDGMENT

The authors thank Israel Wachs for the preparation of the passivated iron powder used in this study. We also acknowledge L. E. McCandlish and C. Mims for their helpful discussions.

REFERENCES

1. Fischer, F., and Tropsch, H., *Brennst.-Chem.* **4,** 276 (1923).
2. Frohning, C. D., Kobel, H., Ralek, M., Rottig, W., Schnur, F., and Schulz, H., *in* "Chemiesohstoffe aus Kohle" (J. Falbe, Ed.), Chap. 8. Stuttgart, 1977.
3. Dry, M. E., Du Plessis, J. A. K., and Leuteritz, G. M., *J. Catal.* **6,** 194 (1966).
4. Shultz, J. F., Hofer, L. E., Stein, K. C., and Anderson, R. B., *Bur. Mines Bull.* 612 (1963).
5. Storch, Golumbic, and Anderson, "The Fischer–Tropsch and Related Synthesis." Wiley, New York, 1951.
6. Raupp, G. B., and Delgass, W. N., *J. Catal.* **58,** 361 (1979).
7. Niemantsverdriet, J. W., van der Kraan, A. M., van Dijk, W. L., and van der Baan, H. S., *J. Phys. Chem.* **84,** 3363 (1980).
8. Reymond, J. P., Meriaudeau, P., and Teichner, S. J., *J. Catal.* **75,** 39 (1982).
9. Krebs, H. J., Bonzel, H. P., and Gafner, G., *Surface Sci.* **88,** 269 (1979).
10. Dwyer, D. J., and Somorjai, G. A., *J. Catal.* **52,** 291 (1978).
11. Bonzel, H. P., and Krebs, H. J., *Surface Sci.* **91,** 499 (1980).
12. Bonzel, H. P., and Krebs, H. J., *Surface Sci.* **117,** 639 (1982).
13. Krebs, H. J., Bonzel, H. P., Sebwarting, W., and Gafner, G., *J. Catal.* **72,** 199 (1981).
14. Goodman, D. W., Kelly, R. D., Madey, T. E., and Yates, J. T., *J. Catal.* **63,** 226 (1980).
15. Bonzel, H. P., *Chem. Ing. Tech.* **54,** 908 (1982).
16. Hardenbergh, J. H., and Dwyer, D. J., *J. Vac. Sci.*, submitted.
17. Vannice, M. A., *J. Catal.* **37,** 449 (1975).
18. Textor, M., Gay, I. D., and Mason, R., *Proc. Roy. Soc. (London)* **A356,** 37 (1977).
19. Hirohawa, K., and Okee, H., *Talanta* **26,** 855 (1979).
20. Henrici-Olive', G., and Olive', S., *Angew. Chem.* **88,** 144 (1976).
21. Satterfield, C. N., and Huff, G. A., *J. Catal.* **73,** 187 (1982).

22. Fischer, F., and Tropsch, H., *Brennst.-Chem.* **7,** 97 (1926).
23. Araki, M., and Ponec, V., *J. Catal.* **44,** 439 (1976).
24. Biloen, P., Helle, J. N., and Sachtler, W. M. H., *J. Catal.* **58,** 95 (1979).
25. Brady, R. C., and Pettit, R., *J. Amer. Chem. Soc.* **102,** 6181 (1980).
26. Brady, R. C., and Pettit, R., *J. Amer. Chem. Soc.* **103,** 1287 (1981).
27. Biloen, P., and Sachtler, W. M. H., *Advan. Catal.* **30,** 165 (1981).
28. Niemantsverdriet, J. W., and van der Kraan, A. M., *J. Catal.* **72,** 385 (1981).
29. Raupp, G. B., and Delgass, W. N., *J. Catal.* **58,** 348 (1979).